The electronic structures and optical properties of B, C or N doped $BaTiO_3$

Zhuang Teng, Jiajun Jiang, Gaoyuan Chen, Chunlan Ma, and Feiwu Zhang

Citation: AIP Advances **8**, 095216 (2018); doi: 10.1063/1.5047094
View online: https://doi.org/10.1063/1.5047094
View Table of Contents: http://aip.scitation.org/toc/adv/8/9
Published by the American Institute of Physics

The electronic structures and optical properties of B, C or N doped $BaTiO_3$

Zhuang Teng,[1] Jiajun Jiang,[2,3] Gaoyuan Chen,[1] Chunlan Ma,[1] and Feiwu Zhang[1,2,3,a]

[1]*Jiangsu Key Laboratory of Micro and Nano Heat Fluid Flow Technology and Energy Application, School of Mathematics and Physics, Suzhou University of Science and Technology, Suzhou, Jiangsu 215009, China*
[2]*State Key Laboratory of Ore Deposit Geochemistry, Institute of Geochemistry, Chinese Academy of Sciences, Guiyang 550081, China*
[3]*Key Laboratory of Earth and Planetary Physics, Institute of Geology and Geophysics, Chinese Academy of Sciences, Beijing 100029, China*

(Received 5 July 2018; accepted 5 September 2018; published online 18 September 2018)

The electronic structures and optical properties of Boron, Carbon or Nitrogen doped $BaTiO_3$ are calculated by the first-principles calculations. The doped atoms decrease the band gap of $BaTiO_3$ significantly, which could increase the host material ability to absorb the visible light. The absorption spectrum calculations confirm that both Boron and Carbon-doped $BaTiO_3$ have a favorable performance in the absorption of visible light. However, Nitrogen-doped $BaTiO_3$ doesn't present the improvement. $BaTiO_3$ doped with Boron or Carbon is expected to be a new class of perovskite materials for the field of solar energy. https://doi.org/10.1063/1.5047094

Solar energy is an abundant and clean source of power and the development and utilization of solar energy have attracted the great interest. In a general way, the use of solar energy can be done in two aspects. One is transforming solar energy into thermal energy (the thermoelectric conversion principle), and the other way is to convert it into electricity directly (the photoelectric conversion principle). The solar cell plays an essential role in the latter case. However, the total electricity of solar power in the whole world takes up a very small proportion at present, mainly due to the low transformation efficiency of the photovoltaic device. Therefore, developing more efficient photovoltaic materials has become an urgent matter in the solar power industry.

The efficiency of photoelectric conversion, which is mainly based on the spontaneous polarization characteristics[1,2] is found in a variety of ferroelectrics.[3,4] The ferroelectric materials with the ABO_3 type perovskite structure have been widely used in photovoltaic industries due to their unique structures.[5–8] The research group Park in Korea reported that their transfer efficiency of the perovskite photovoltaic device was 6.5% in 2011.[9] While Snaith et al. reported a value of 15.9%[10] in 2012. Ferroelectric photovoltaic materials have a peculiar property that the direction of polarization can be changed by applying an electric field. Ferroelectric photovoltaic materials of perovskite-type oxides have been widely studied at present, which includes at least $LiNbO_3$,[11–14] $BaTiO_3$,[11] and $BiFeO_3$,[15] etc.

$BaTiO_3$ is one of the most typical ABO_3 perovskite oxide material. It has a tetragonal phase at room temperature, and the reason of its spontaneous polarization is that the Ti atom deviates from the center of the oxygen octahedron, causing displacement along the direction of the fourfold axis. The internal electric field caused by spontaneous polarization can separate the photogenerated electron-hole pair preventing them from recombination. This mechanism is beneficial to the storage of solar energy. However, $BaTiO_3$ has a large band gap (3.4 eV by experimental measurements[16])

[a]E-mail: zhangfeiwu@usts.edu.cn

which makes it difficult to absorb the energy of the visible light effectively (1.4~2.0 eV). Fortunately, both theoretical and experimental studies have shown that the band gap can be regulated by doping impurities. The idea is that if the band gap of $BaTiO_3$ can decrease to the visible light level by introducing impurity atoms in the lattice, we may provide the theoretical guidance on the materials which can be used as the solar cell. In 2012, the group of C. Gruber[17] replaced one oxygen atom by B, C or N atom in cubic $BaTiO_3$, and they found that *p*-element-doped perovskites could provide a new class of materials for magneto-optics. Motivated by this work, we here simulated the tetragonal $BaTiO_3$ doped with Boron, Carbon or Nitrogen atom and calculated their band gaps and optical properties.

We perform the calculation by using the projector augmented wave method (PAW)[18,19] based on the density functional theory (DFT) by the *Vienna ab initio simulation package* (VASP).[20] A generalized gradient approximation (GGA) has been used for the exchange and correlation. We take the 2×2×2 supercell with a tetragonal phase of 40 atoms to perform our calculations, see Fig. 1(a). The experimental value of the lattice constant $a = b = 3.992$ Å, $c = 4.036$ Å[21] are set as the initial lattice constant. The convergence tests have approved the cutoff energy of 500 eV, and a 6×6×6 Monkhorst-Pack K mesh for the Brillouin-zone integration is enough for our calculations. The optimization, including the atomic position and lattice constants, is performed until all the force components are less than 0.01 eV/Å. Due to the GGA within DFT are poor at accurately calculating band gaps, the hybrid functional in HSE06 version has also been employed to calculate the bulk $BaTiO_3$. We introduce one Boron, Carbon or Nitrogen impurity atom in the lattice to substitute an oxygen atom, respectively. The dopant concentration is 2.5%. The density of states (DOS), band structure and optical properties are calculated after the full structure relaxation. There are three different oxygen atom sites in the $BaTiO_3$ unit cell. We have modeled all the doping configurations and compared their defect formation energies to determine their stabilities.

The total free energies of the supercells with one oxygen (O1, O2 or O3) replaced by *X* atom (*X*=B, C or N) are calculated to determine which oxygen site substitution mechanism is the most energetically favorable. We find all three impurity atoms (B, C, and N) have a lower total free energy at the O2 site than the other oxygen sites. Therefore, the band structures and density of states are calculated with the impurity atom *X* substitution at the O2 site. The supercell structure and the position of *X* are shown in Fig. 1.

Replacing one oxygen breaks the tetragonal symmetry of the supercell. The cell volume and the distance between Ti and dopant atom *X* (*X* = Boron, Carbon or Nitrogen) are changed compared with the pure $BaTiO_3$. A summary of the calculated results is shown in Table I.

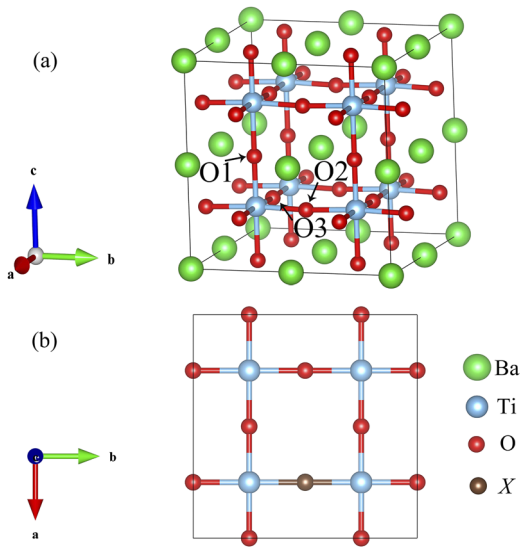

FIG. 1. The $BaTiO_3$ structure (a) and the position of the impurity atom X (X= Boron, Carbon or Nitrogen) in the BaTiO3 lattice (b).

TABLE I. The relaxed BTO:*X* (*X* = B, C, N) and BTO lattice parameters: cell volume, *c*/*a* and *b*/*a* ratio, the magnetic moment, the distance between Ti and *X* atoms and the band gap.

	BTO	BTO:B	BTO:C	BTO:N
Cell Volume (Å^3)	67.29	69.50	68.11	68.09
c/*a*	1.046	1.090	1.052	1.070
b/*a*	1	1.019	1.011	1.005
M(μ_B)	0	1	2	1
$d_{Ti\text{-}X}$ (Å)	2.012	2.189	2.116	2.033
GAP-GGA (eV)	1.70	0.48	0.86	0.55
GAP-correction (eV)	3.20[a]	1.98	2.36	2.05

[a]This value is calculated by HSE06. The rests are difference corrections between GGA and HSE06.

The total density of states (TDOS) nearing Fermi level for doped and undoped $BaTiO_3$ is shown in Fig. 2. The GGA calculated band gap of the pure $BaTiO_3$ is 1.70 eV, and the HSE06 calculated value is 3.20 eV, which is the same as the results of Gruber.[17] We should point out that the difference between the DFT calculated band gap with the experimental value is due to the well-known deficiencies of DFT calculations in determining the band gap. Both local density approximation (LDA) and GGA methods underestimate the band gap in both semiconductors and insulators calculations. Although the GGA method normally underestimates the band gap of $BaTiO_3$, it could give a reliable tendency of the band gap change with the structure and composition change. When the oxygen atom is replaced by B, C or N impurity atom in the lattice, the band gap decreases to a different degree. For BTO:C ($BaTiO_3$ doped with Carbon atom), it has reduced to 0.86 eV, which is beneficial to the absorption of the visible light. However, it appears a tiny impurity state is nearing Fermi level for BTO:B ($BaTiO_3$ doped with Boron atom) and BTO:N ($BaTiO_3$ doped with Nitrogen atom).

In the Boron atom doped BTO lattice, we find a tiny impurity state just beneath the Fermi level which decreases the band gap. This impurity state mainly comes from the interaction of B 2*p* states and Ti 3*d* states. For Ba atoms, they almost do not influence the density of states nearby the Fermi level. For Ti atoms, both *s* and *p* orbitals are becoming occupied, leaving an empty 3*d* state. For O atoms, all the orbitals are occupied, each of the two adjacent Ti atoms gives the oxygen one electron, forming a stable occupied state of O 2*p*. For B atom, both the spin up and spin down states form two peaks at the bottom and the top of the gap. Each of the two adjacent Ti atoms also gives one electron to boron atoms forming a covalent bond as performed by the oxygen atom in the pure lattice. In the

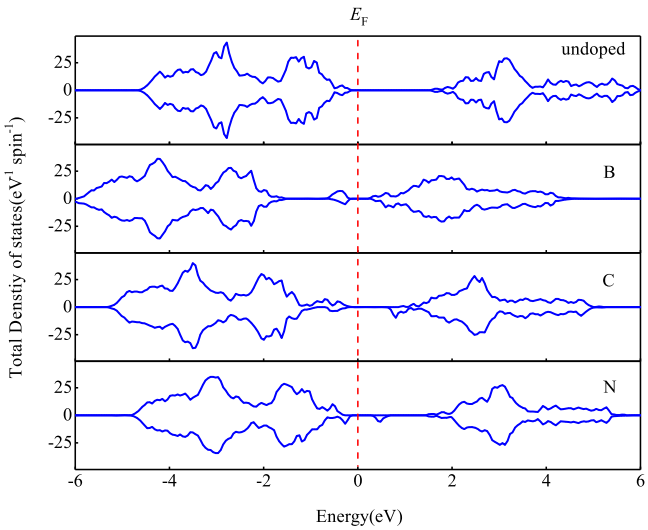

FIG. 2. The total density of states (TDOS) nearing Fermi level (E_F) for undoped pure and Boron, Carbon and Nitrogen doped $BaTiO_3$.

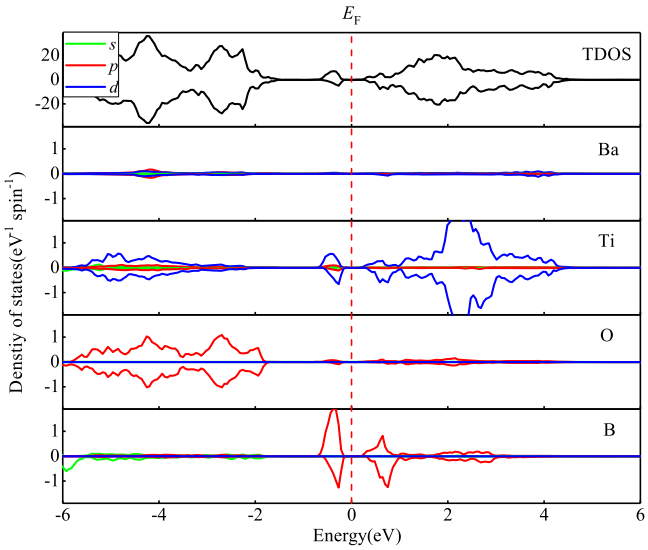

FIG. 3. The density of states (DOS) of *s*, *p* and *d* orbitals of each atom in BTO:B.

B doped lattice, the B 2*p* orbital has three electrons, two spin up and one spin down, which forms a magnetic moment of 1 μ_B, which has been observed in our BTO:B calculations. The density of states for $BaTiO_3$ doped with Boron atom is shown in Fig. 3.

In the C atom doped BTO lattice, our calculations show that the tiny impurity state nearby Fermi level disappears and the band gap decreases to 0.86 eV. This is a significant drop compared to the undoped pure state. The Ba atoms have no contribution to the density of states nearby the Fermi level. As shown in the BTO:B lattice, the outermost orbital is unoccupied for Ti and fully occupied for O. However, there is one more electron in the carbon *p* orbital than in boron. Three of the carbon p orbital electrons are spin up, which forms a peak at the bottom of the band gap. The rest one p orbital electron is spin down, leaving two unoccupied spin down orbitals, which causes two peaks distributing at each side of the Fermi level. The net magnetic moment is 2 μ_B.

We have also found a magnetic moment of 2 μ_B in our calculations. The density of states for $BaTiO_3$ doped with Carbon atom is shown in Fig. 4.

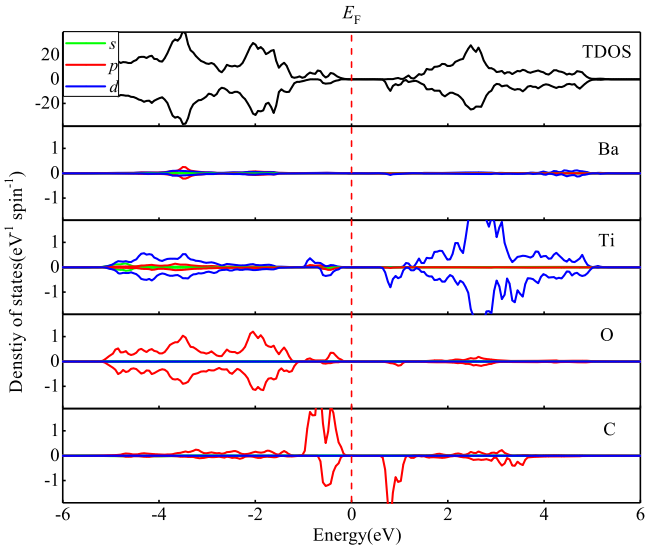

FIG. 4. The density of states (DOS) of *s*, *p* and *d* orbitals of each atom in BTO:C.

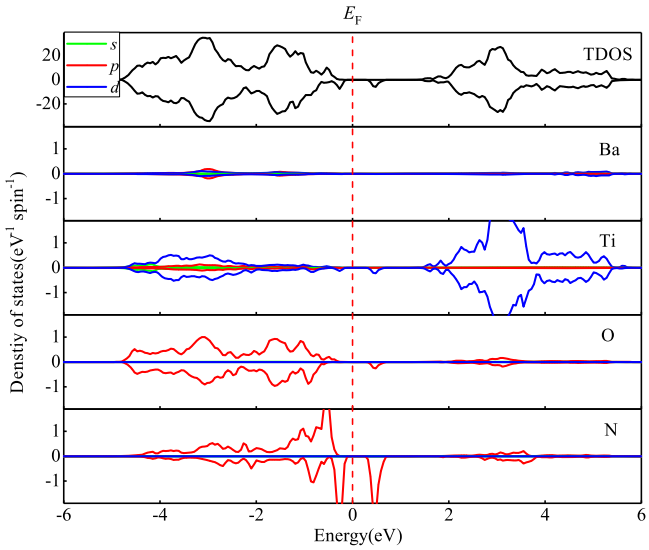

FIG. 5. The density of states (DOS) of *s*, *p* and *d* orbitals of each atom in BTO:N.

There appeared a tiny impurity state in the middle of the band gap, which is similar to the B doped case when using N atom to replace one oxygen. This impurity state mainly comes from the N 2*p* electrons. The Ba, Ti, and O atoms almost have the same electronic structures and properties compared with BTO:B and BTO:C respectively. The Ti 3*d* orbitals are unoccupied, and the O 2*p* orbitals are occupied. The difference lies in the magnetic moment of the *p*-electron. Since nitrogen has one more electron than carbon, three electrons occupy the spin up orbitals, and two electrons spin down, forming a magnetic moment of 1 μ_B. The density of states for $BaTiO_3$ doped with Nitrogen atom is shown in Fig. 5.

For a better understanding of the electronic distribution, we have plotted the electron localization distributions of $BaTiO_3$ doped with Boron, Carbon or Nitrogen in Fig. 6. The plane is cut from Ti-O layer along [001] direction. The cool tone color represents none electronic distribution, while the warm tone represents the existence of electrons. The warm tone colors distribute around O and *X* (*X* = B, C, N) atoms, which indicates that the electrons are localized distribution.

The calculated band structures nearing Fermi level of the doped and undoped $BaTiO_3$ are shown in Fig. 7. The high symmetry points are obtained from Ref. 22. The maximum of the valence band and the minimum of the conduction band of the pure $BaTiO_3$ shown in Fig. 7(a) are located at the A point and the Γ point, forming a band gap of 1.70 eV, which indicates that the pure $BaTiO_3$ is an indirect band gap material. The band gap of the $BaTiO_3$ doped with Boron atom is calculated to be 0.48 eV from Y point of the top of the valence band to T point of the bottom of the conduction band. Three

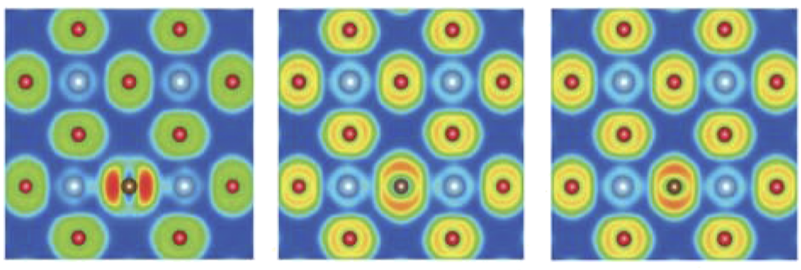

FIG. 6. The electron localization function (ELF) in the (001) plane of (a) BTO:B, (b) BTO:C, and (c) BTO:N.

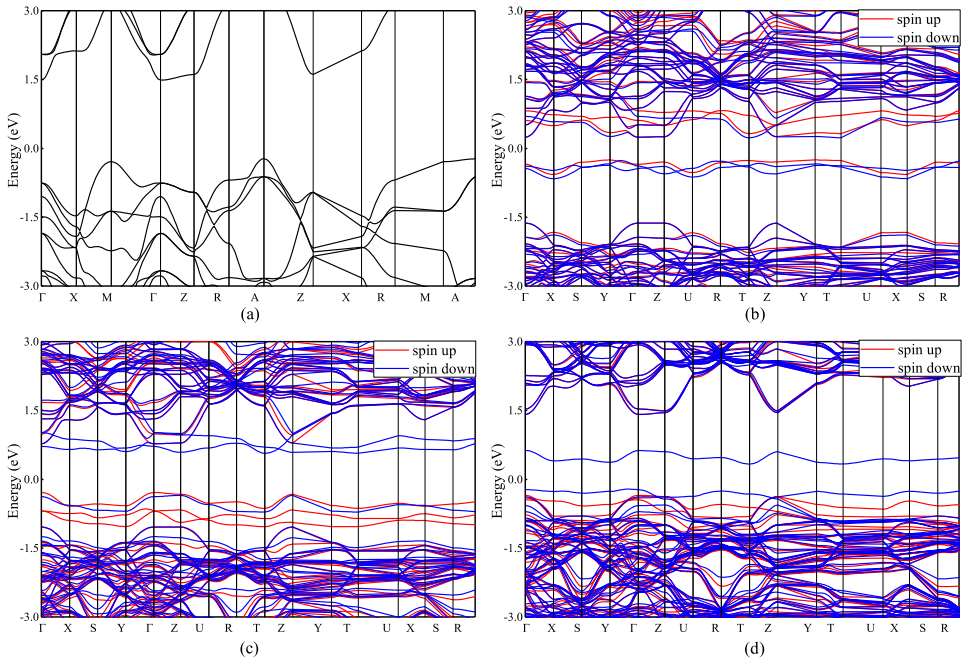

FIG. 7. The band structures of undoped and doped $BaTiO_3$. (a) pure $BaTiO_3$, (b) BTO:B, (c) BTO:C, (d) BTO:N.

impurity bands from B 2*p* states, one spins up and two spin down just under the Fermi level contribute to the diminution of the band gap. Both C and N substitution have the same indirect band structures from Γ point to T point but with different band gap. The values of the gap for C and N doping are 0.86 eV and 0.55 eV respectively, which are in line with the density of states in Fig. 4 and Fig. 5. C 2*p* states in BTO:C distribute at the two sides of Fermi level, replacing the bottom of the conduction band and the top of the valence band respectively. Compared to BTO:B, BTO:N also has impurity states sitting near the Fermi level, with a fewer number of bands, which has only one down spin state in the band gap.

From the above analysis, we know that these three substitutions can adjust the band gap effectively, in addition, the values of the gap are decreased with different degrees which are in favor of the absorption of the visible lights.

The optical properties of the supercell can be determined by the complex dielectric function $\varepsilon(\omega)= \varepsilon_1(\omega)+i\varepsilon_2(\omega)$, where the ε_1 and ε_2 are the real part and the imaginary part of the dielectric function, respectively. The imaginary part is determined by a summation over empty states using the equation:[23]

$$\varepsilon^{(2)}_{\alpha\beta}(\omega) = \frac{4\pi^2 e^2}{\Omega} \lim_{q\to 0} \frac{1}{q^2} \sum_{c,v,\mathrm{k}} 2\omega_{\mathrm{k}} \delta(\varepsilon_{c\mathrm{k}} - \varepsilon_{v\mathrm{k}} - \omega) \times \left\langle u_{c\mathrm{k}+e_\alpha q} | u_{v\mathrm{k}} \right\rangle \left\langle u_{c\mathrm{k}+e_\beta q} | u_{v\mathrm{k}} \right\rangle^*, \tag{1}$$

where the indices c and v refer to conduction and valence band states respectively, $u_{c\mathrm{k}}$ is the cell periodic part of the orbitals at the k-point k, e is the electronic charge, Ω is the volume and ω is the light frequency. The real part of the dielectric function can be derived from the imaginary part using the Kramers-Kronig relations:

$$\varepsilon^{(1)}_{\alpha\beta}(\omega) = 1 + \frac{2}{\pi} P \int_0^\infty \frac{\varepsilon^{(2)}_{\alpha\beta}(\omega')\omega'}{\omega'^2 - \omega^2 + i\eta} d\omega', \tag{2}$$

where P denotes the principal value, see Ref. 23 for more information. According to the real part and the imaginary part of the dielectric function, the primary optical properties such as the refractive index $n(\omega)$, the absorption coefficient $I(\omega)$ can be obtained from the following expressions:[24,25]

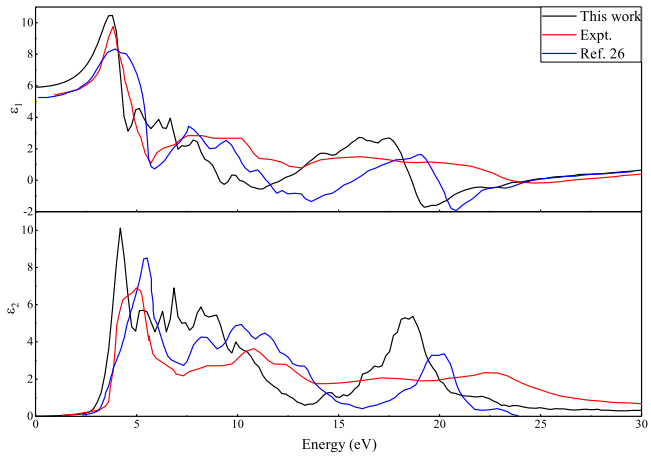

FIG. 8. The calculated real part $\varepsilon_1(\omega)$ (up panel) and the imaginary part $\varepsilon_2(\omega)$ (down panel) of the dielectric function in pure $BaTiO_3$, compared with previous experimental and theoretical results.

$$n(\omega) = \frac{1}{\sqrt{2}}\left\{\left[\varepsilon_1^2(\omega) + \varepsilon_2^2(\omega)\right]^{\frac{1}{2}} + \varepsilon_1(\omega)\right\}^{\frac{1}{2}}, \tag{3}$$

$$I(\omega) = \frac{\sqrt{2}\omega}{c}\left\{\left[\varepsilon_1^2(\omega) + \varepsilon_2^2(\omega)\right]^{\frac{1}{2}} - \varepsilon_1(\omega)\right\}^{\frac{1}{2}}. \tag{4}$$

The real part $\varepsilon_1(\omega)$ and the imaginary part $\varepsilon_2(\omega)$ of the dielectric function for the undoped $BaTiO_3$ are calculated in Fig. 8. As seen in this figure, our results are in good agreement with Zhen Yin's work,[26] as well as the experimental results.[27] In the low-frequency range, there appeared a peak at about 3.7 eV for $\varepsilon_1(\omega)$ for all the three lines. In the range of 1.5~5.0 eV, the imaginary part $\varepsilon_2(\omega)$ rises up quickly, corresponding to the range of intrinsic absorption.

The absorption coefficient $I(\omega)$ for pure and doped $BaTiO_3$ is calculated according to the expression (4), the results are shown in Fig. 9. For clearly understanding the absorption properties in visible light (390~780 nm), we convert the energy into wavelength. The absorption ability is enhanced naturally for BTO:B and BTO:C compared to the pure $BaTiO_3$ in the range of visible light. However, there are almost no changes for BTO:N compared to pure BTO, although BTO:N has decreased the band gap to a large extent like BTO:B and BTO:C. From the band structures in Fig. 7, we find that BTO:N has a fewer number of bands in the impurity states than BTO:B in spite of the same band structure for both of them, which indicates that BTO:N cannot absorb the visible light effectively. There are two peaks for BTO:B at 425 nm and 660 nm, corresponding the two gaps from -1.63 eV

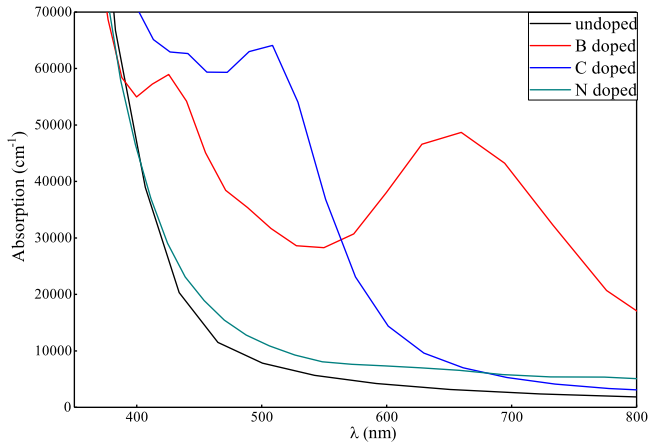

FIG. 9. The absorption coefficient $I(\omega)$ for pure and doped $BaTiO_3$.

to 0.23 eV in Fig. 7(b). Only one peak appears for BTO:C at 508 nm, which is in line with the band gap from -0.29 eV to 0.57 eV in Fig. 7(c). BTO:B has a broader range of absorption compared to BTO:C. Both BTO:B and BTO:C have a good performance in the absorption of visible light.

CONCLUSIONS

We have calculated the electronic structures, band structures and optical properties of $BaTiO_3$ doped with Boron, Carbon or Nitrogen atoms by using density functional theory. We can confirm the band gap will be efficiently changed by introducing the impurities into the lattice for the solar industry application purpose. When the foreign atoms (Boron or Nitrogen) is introduced into the BTO lattice, there appears a tiny impurity state nearby the Fermi level, causing the band gap decreases. For C doping, C 2*p* states replace both the bottom of the conduction band and the top of the valence band in $BaTiO_3$, which decreases the band gap primarily so that it can absorb the visible light. The simulated absorption spectrums predict that BTO:B and BTO:C are able to absorb the visible light effectively, which can be evidenced by the two peaks or the one peak in the absorption spectrums of the B and C bearing systems. However, the peak is not observed in the absorption spectrum of BTO:N. In order to test the impurities concentration effect, we have also calculated the 3×3×3 supercell with 135 atoms with lower impurity concentrations (0.74%), which doesn't change our conclusion of this report. Our theoretical calculations may play a significant guide role in photovoltaic materials design and its application predictions.

ACKNOWLEDGMENTS

T. Zhuang thanks Wei Xun for fruitful discussion and computational facility support. This work is supported by National Natural Science Foundation of China (11304218, 11247023, 41773057), and NSF of Jiangsu Higher Education Institutions (No. 17KJA140001). Thanks for the support of the Recruitment Program of Chinese thousand-talents scheme.

[1] L. Pintilie, I. Vrejoiu, G. L. Rhun, and M. Alexe, "Short-circuit photocurrent in epitaxial lead zirconate-titanate thin films," J. Appl. Phys. **101**, 064109 (2007).
[2] V. M. Fridkin, "Bulk photovoltaic effect in noncentrosymmetric crystals," Crystallography Reports **46**, 654–658 (2001).
[3] R. V. Baltz, "Theory of the anomalous bulk photovoltaic effect in ferroelectrics," Phys. Status Solidi **89**, 419–429 (1978).
[4] A. G. Chynoweth, "Surface space-charge layers in barium titanate," Phys. Rev. **102**, 705–714 (1956).
[5] J. F. Scott, C. A. Araujo, B. M. Melnick, L. D. Mcmillan, and R. Zuleeg, "Quantitative measurement of space-charge effects in lead zirconate-titanate memories," J. Appl. Phys. **70**, 382–388 (1991).
[6] H. P. Rooksby, "Compounds of the structural type of calcium tianate," Nature **155**, 484 (1945).
[7] X. Zhang, Z. M. Xiu, and X. W. Li, "Preparation and characterization of (HAp/SiO_2)/Ti biocomposites," Advanced Materials Research **217-218**, 88–92 (2011).
[8] J. Zhuang, G. S. Li, X. C. Gao, X. B. Guo, Y. H. Huang, Z. Z. Shi, Y. Y. Weng, and J. Lu, "Preparation and photorefractive properties of barium strontium titanate ($Ba_{1-x}Sr_xTiO_3$)," Opt. Commun. **82**, 69–72 (1991).
[9] J. H. Im, C. R. Lee, J. W. Lee, S. W. Park, and N. G. Park, "6.5% efficient perovskite quantum-dot-sensitized solar cell," Nanoscale **3**, 4088–4093 (2011).
[10] B. E. Hardin, H. J. Snaith, and M. D. Mcgehee, "The renaissance of dye-sensitized solar cells," Nat. Photonics **6**, 162–169 (2012).
[11] L. Arizmendi, "Photonic applications of lithium niobate crystals," Phys. Status Solidi. **201**, 253–283 (2004).
[12] V. M. Fridkin and B. N. Popov, "Anomalous photovoltaic effect in ferroelectrics," Sov. Phys. Usp. **126**, 657–671 (1978).
[13] A. M. Glass, D. Von der Linde, and T. J. Negran, "Highvoltage bulk photovoltaic effect and the photorefractive process in $LiNbO_3$," Appl. Phys. Lett. **25**, 233–235 (1974).
[14] A. M. Glass, D. V. D. Linde, D. H. Auston, and T. J. Negran, "Excited state polarization, bulk photovoltaic effect and the photorefractive effect in electrically polarized media," J. Electron. Mater. **4**, 915–943 (1975).
[15] M. M. Kumar, V. R. Palkar, K. Srinivas, and S. V. Suryanarayana, "Ferroelectricity in a pure $BiFeO_3$ ceramic," Appl. Phys. Lett. **76**, 2764–2766 (2000).
[16] S. H. Wemple, "Polarization fluctuations and the optical-absorption edge in $BaTiO_3$," Phys. Rev. B **2**, 2679–2689 (1970).
[17] C. Gruber, P. O. Bedollavelazquez, J. Redinger, P. Mohn, and M. Marsman, "p-electron magnetism in doped $BaTiO_{3-x}M_x$ (M=C, N, B)," Europhys. Lett. **97**, 67008 (2012).
[18] P. E. Blöchl, "Projector augmented-wave method," Phys. Rev. B **50**, 17953–17979 (1994).
[19] G. Kresse and D. Joubert, "From ultrasoft pseudopotentials to the projector augmented-wave method," Phys. Rev. B **59**, 1758–1774 (1999).
[20] G. Kresse and J. Furthmüller, "Efficient iterative schemes for ab initio total-energy calculations using a plane-wave basis set," Phys. Rev. B Condensed Matter **54**, 11169–11186 (1996).
[21] T. Mitsui, *Oxides* (Springer, Berlin Heidelberg, 1981).

[22] W. Setyawan and S. Curtarolo, "High-throughput electronic band structure calculations: Challenges and tools," Comput. Mater. Sci. **49**, 299–312 (2010).
[23] M. Gajdoš, K. Hummer, G. Kresse, J. Furthmüller, and F. Bechstedt, "Linear optical properties in the projector-augmented wave methodology," Phys. Rev. B **73**, 045112 (2006).
[24] S. Saha, T. P. Sinha, and A. Mookerjee, "Electronic structure, chemical bonding, and optical properties of paraelectric $BaTiO_3$," Phys. Rev. B **62**, 8828–8834 (2000).
[25] C. Samantaray, H. Sim, and H. Hwang, "First-principles study of electronic structure and optical properties of barium strontium titanates ($Ba_xSr_{1-x}TiO_3$)," Appl. Surf. Sci. **250**, 146–151 (2005).
[26] M. Q. Cai, Z. Yin, and M. S. Zhang, "First-principles study of optical properties of barium titanate," Appl. Phys. Lett. **83**, 2805–2807 (2003).
[27] D. Bäuerle, W. Braun, V. Saile, G. Sprüssel, and E. Koch, "Vacuum ultraviolet reflectivity and band structure of $SrTiO_3$ and $BaTiO_3$," Zeitschrift für Physik B Condensed Matter **29**, 179–184 (1978).